Article citation info:
Ameen KA, Hussein ZA. Stress redistribution and relocation using auxiliary holes in perforated plates under tensile loading. Diagnostyka. 2026;27(3):2026310. https://doi.org/10.29354/diag/231659.



**DIAGNOSTYKA**, 2026, Vol. 27, No. 3

**e-ISSN** 2449-5220
**DOI:** 10.29354/diag/231659

# STRESS REDISTRIBUTION AND RELOCATION USING AUXILIARY HOLES IN PERFORATED PLATES UNDER TENSILE LOADING

**Kayser Aziz AMEEN, Zaid Ali HUSSEIN ***

College of Mechanical Engineering, University of Technology - Iraq, Baghdad, Iraq
* Corresponding author, e-mail: zaid.a.hussien@uotechnology.edu.iq

Abstract

The effect of auxiliary relief holes on the stress redistribution in a thin plate with holes subjected to uniaxial tensile loading is investigated. A finite element model was implemented in ANSYS APDL for the plate with a central circular hole and other secondary-hole patterns. This included number of auxiliary holes, angular distributions and distances from the main hole. Results are checked from the perspective of maximum von Mises stress, principal stress, shear load, strain energy density, total deformation and stiffness/weight reduction/factor of safety/stress concentration factor. The global elastic response of the numerical model was validated using experimental tensile testing of the baseline specimen. The results demonstrate that local stress is either relieved or intensified depending on the arrangement of auxiliary holes. The stress concentration due to overlapping stress fields is more significant for the configurations with unfavourable angular spacing and ligament interaction (B24 and B34). However, model B42 showed the best combination between stress concentration, safety factor, stiffness retention and weight reduction with: Stress concentration factor = 4.304; Safety factor = 23.23. Though peak stress reduction was marginal, the optimal configuration moved peak stress significantly while introducing little to no loss in global stiffness. These results highlight that auxiliary-hole design should focus on geometric optimization instead of a mere increase in the number of holes. The research serves as a helpful reference for the fatigue design of lightweight perforated structures with stress control and structural assurance.

Keywords: factor of safety, finite element method, strain energy density, stress redistribution, Von Mises stress

## 1. INTRODUCTION

Perforated elements with different geometric discontinuities (e.g., circular, elliptical or rectangular holes) are commonly used as engineering structures to meet functional purposes such as reduction of weight, ventilation and passage. The presence of such openings, however, introduces local disturbances to the internal trajectories of stress and causes intense stress concentration zones. Under the application of uniaxial tensile loading, it is known that localized stress (which arises in the vicinity of these discontinuities) can increase multiple times, upwards of an order greater than its nominal applied value. This specific form of damage, defined by the Stress Concentration Factor (Kt), facilitates micro-crack nucleation, fatigue failure and eventually multiscale structural rupture. Therefore, minimizing stress concentration around complex geometric cutouts without an effective change in their structural behavior or a shift from the baseline geometry continues to be a major engineering challenge for mechanical structural designers.

In the past, several approaches have been suggested to overcome stress concentrations, including optimized hole profiles and composite reinforcements. Out of the discussed techniques, secondary auxiliary holes are one of the most efficient passive safe and economical optimization approaches implemented as stress-relief or relief holes. In planned auxiliary holes adjacent to the main opening, they guide and redistribute stress trajectories in a smooth manner which further lowers peak stress magnitude at the critical boundary.

### 1.1. Literature review

Many researchers have looked into optimizing the bearing ability of perforated structures through holes in the structure. Investigating the stress concentration reduction effect of using auxiliary holes, which was highlighted by [1], shows that with a proper configuration design principles for auxiliary holes, the material flow lines around primary circular cutouts in plate configurations become sufficiently smooth and uniform. We performed a parametric optimization of the mitigation of stress concentration in plates with central oblique elliptical holes by means of auxiliary circular holes [2]. They found

Received 2026-06-28; Accepted 2026-08-24; Available online 2026-08-25

that the separation distance between primary and secondary orifices was a key factor in stress mitigation. Originally, Cannarozzi and Molari [3] used finite element analysis (FEA) to study of stress concentration factor on a perforated plates under tensile load with the auxiliary hole diameters as the main variable. Birn et al. [4] investigated optimization of holes in plates subjected to bi-axial load and proved it through the response of surrounding stress fields that interact either decrease or increase local stresses depending on geometric orientation.

In addition, Hou et al. [5] compared circular and elliptical auxiliary openings to emphasize that under certain directional loadings, elliptical relief holes can provide effective mitigation. More recently, Khaja et al. [6] studied the effect of clustered micro-relief holes on mitigating stress concentrations in tensioned plates and suggested some first steps regarding the required net ligament widths to prevent unwanted interactions. Similar stress-relief and stress-reduction concepts have also been applied in mechanical components such as spur gears, where circular, elliptical, and optimized auxiliary features were introduced to reduce local stress concentration and improve load distribution [7, 8]. In perforated plates and finite-width structural members, previous analytical and numerical studies showed that hole diameter, ligament width, plate geometry, boundary conditions, and material distribution strongly affect the stress concentration factor and the resulting mechanical response [9-12]. Furthermore, investigations on optimized perforated and composite structural components confirmed that the position and interaction of neighbouring holes can relocate the maximum stress zone and may either reduce or amplify local stress depending on the spacing and loading direction [13-15]. Recently, researchers integrated numerical tools for topology optimization; in reference [16], the author presented a methodology to optimize the structural topology using optimality criteria. In recent years, perforated and custom-shaped geometries have been increasingly employed in thermal, energy, and vibration-sensitive mechanical systems due to their significant influence on transport performance, structural response, and mechanical reliability [17-22]. Flow-induced vibrations, a type of vibrational phenomenon caused by fluid motion. In general, the study of system structures influences the efficiency of the components that constitute those systems [23-24].

### 1.2. Research gap

Existing literature has extensively documented the use of symmetric pairs or simple linear arrays of defense holes, but no thorough investigation on multi-hole secondary designs in intricate angular patterns relative to a primary circular cutout has yet been performed. Most previous models are limited by two or four additional holes with an exact configuration following the loading axes. Interaction effects of varying both the radial distance and angular density of up to (9) secondary holes remain largely stoichiometric. Importantly, the boundary transition between auxiliary holes which serve as 'stress-relief zones' and those that act as 'stress-amplification zones' because of their field overlap has not yet been systematically quantified.

### 1.3. Research objectives

In order to overcome these limitations, this work provides a methodical numerical and experimental characterization of the structural behavior of holes in thin steel plates subjected to uniaxial tensile loading. The primary objectives are:

- Using ANSYS APDL to model and analyze a wide parametric array of auxiliary hole configurations (hole count, angular spacing, and radial offsets).
- For quantifying the differences in Von Miss stress, principal stress, strain energy density and global structural stiffness between varying geometric topologies.
- Step two is physical, experimental tensile testing to assess the finite element models created and validate numerical predictions.
- To develop a finite element model of the baseline specimen and validate against tensile testing before using that validated numerical model to create parametric models for the auxiliary-hole configurations.
- Secondary holes are used to change and rearrange stress trajectories surrounding the main hole so that when located in a passive area, they can diminish localized stress concentration and translate the critical stress point while preserving the general rigidity of the piece.

### 1.4. Research novelty

The original novelty and contribution of this research is that maximal stress field are strategically relocated from conventional stress-rank boundaries (circular holes circular)" to optimal low stressed boundary points. This strategy is different from the traditional strategies that only try to local minimize the peak stress value, by optimizing specifically for the angular and radial distribution of secondary holes (for instance, configurations such as B42 specified in Table 1) one can safely redistribute a given primary critical stress into net ligament pathways between auxiliary holes. This intentional relocation of the resonant stress peak allows for its main opening to be kept free from premature yielding resulting in a "stress-shielding" effect, improving the effective safety factor (to 23.23) on this critical component while losing structural weight without enlarging its main envelope.

Table 1. The variation in stress with and without the secondary hole

| Model | Stress at Model A (50,15) | Stress at location (50,15) | Stress at new location | New location for max stress |
|---|---|---|---|---|
| B15 | 10.84 | 10.53 | 11.77 | 57.07,17.57 |
| B24 | 10.84 | 10.37 | 13.19 | 57.07,17.57 |
| B34 | 10.84 | 10.18 | 12.97 | 57.07,17.57 |
| C15 | 10.84 | 10.8 | 10.81 | 62.07,17.57 |
| C43 | 10.84 | 11.05 | 12.37 | 63.66,15 |

## 2. MATERIALS AND METHODS

### 2.1. Experimental tensile testing and analytical modeling (model A)

At first, for establishing a reliable baseline, a hybrid experimental and theoretical investigation was performed on the reference specimen Model A which comprises of a solid steel plate that contains only the primary (central) round hole (D = 10 mm) and no secondary hole present.

#### 2.1.1. Experimental setup (static tensile test)

The assumptions for the finite element analysis were as follows:

(1) Since the thickness to width ratio of the steel plate being half is small enough, it was modelled as a two-dimensional plane-stress problem;
(2) The material was modelled as linear elastic;
(3) Small-deformation assumptions were adopted;
Uniaxial Tensile Load of 100 N on the plate
(4) The load was considered to be in the elastic range and did not include any material or geometric nonlinearity. The plate was modelled with the PLANE82 element.

Displacement controlled loading was applied through a computerized Universal Testing Machine (UTM) during a static uniaxial tensile test. The specimen dimensions were in accordance with typical tensile configurations; the specimen was 20 mm wide, 100 mm long and 2 mm thick as illustrated in Figure 1.

The dimension of each specimen as shown in Figure 2 (c) with a centrally pierced circular hole of 10 mm diameter. The material utilized is a structural steel grade with an elastic modulus (E) of 200 GPa and a Poisson's ratio (ν) of 0.3. A nominal tensile force (P) of 100 N was applied axially to the specimen.

All the specimens were machined using Water Jet Cutting (WJC) to ensure precise dimensional accuracy. This technique was adopted because it produces minimal to negligible residual stresses, as it does not introduce thermal or mechanical distortion during the cutting process. Testing was carried out at room temperature (23 ± 2 °C) under displacement-controlled conditions and hydraulic grips were applied to prevent slippage during testing. Since stresses could not be directly measured, longitudinal strain was measured by Universal Testing Machine (UTM) and later converted into stress according to Hooke’s law in the elastic region. The gauge section of the specimen was fitted with a clip-on axial extensometer (gage length: 25 mm, accuracy: ± 1 μm). The extensometer, was complemented before the testing with a standard calibration block and the zero reference was checked for each sample prior to starting test. Local stress concentration was not experimentally measured.

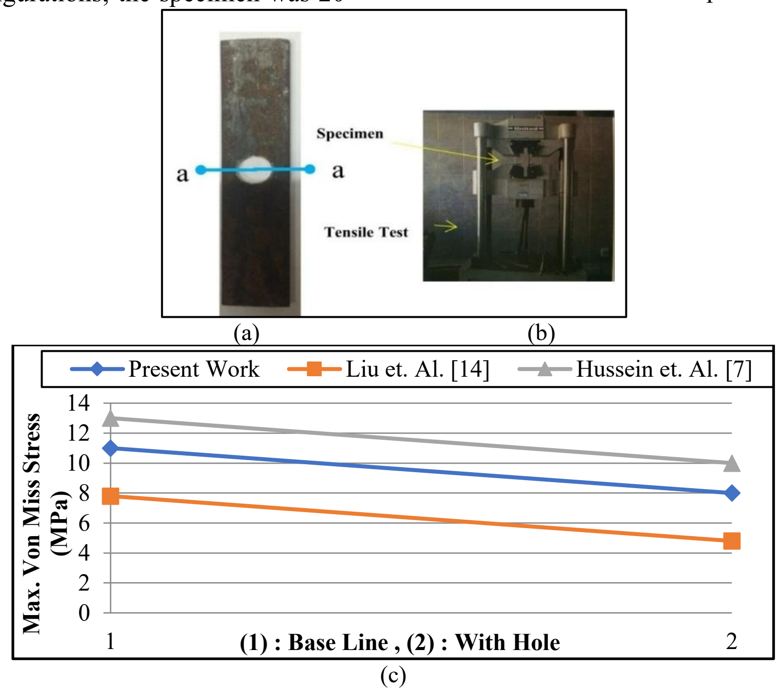


Fig. 1. (a) Geometry of the tested specimen, (b) universal tensile testing machine, (c) comparison of stress Von Miss with auxiliary holes

Because it was not possible to measure directly the stresses imposed in the arms, longitudinal strain was measured using the Universal Testing Machine (UTM) and transformed into stress enforcement according to Hooke's law in the elastic region. This mechanical property was not measured experimentally using local stress concentration. Experimental validation was performed only for the global elastic response of the reference specimen. Experimental validation does not determine any local stress concentration about the hole, and thus consists primarily of material properties governing overall stiffness and elastic behavior.

For the reference specimen (a specimen without secondary perforations), the average stress measured under a tensile load of 100 N was 9.41 ± 1.21 MPa, while the finite element model predicted a value of 10.8 MPa. This discrepancy of approximately 10.2%. Experimental validation was limited to global elastic response due to the difficulty of directly measuring localized stresses near hole boundaries.

**2.1.2. Measurement uncertainty analysis**

In accordance with the Guide to the Expression of Uncertainty in Measurement (GUM), uncertainty assessment was conducted to ascertain the reliability and reproducibility of each experimental measurement. The experimental program included testing eight identical specimens under an Instron 8802 servo-hydraulic Universal Testing Machine with a maximum axial load capability of ±100 kN. The tensile load was exerted in a displacement-controlled way, and the axial deformation was measured with a clip-on extensometer calibrated at the same day.

For the reference specimen, the average stress measured in both cases from eight repeated tests with standard deviation values was 9.41 MPa (SD = ± 1.21 Mpa). The uncertainty in these experimental measurements stems from multiple sources of error, including load-cell accuracy, extensometer resolution, specimen dimensional tolerances, variability in property (material) composition, and repeatability of the experiments.

Statistical evaluation of repeatability from the experimental results indicated that it was the major source of measurement uncertainty. The standard uncertainty of the repeatability was computed by dividing the standard deviation over the square root of number of specimens tested to yield at approximately 0.428 MPa. Furthermore, the uncertainty associated with the load measurement system was calculated based on manufacturer accuracy statement from the Instron 8802 testing machine. Due to the small applied load compared with machine capability, load–cell uncertainty had a negligibility contribution on total measurement uncertainty compared to scatter seen between experimental results.

The root-sum-square (RSS) method was used to evaluate the combined standard uncertainty. The expanded uncertainty was calculated with a coverage factor of k= 2 (approximate confidence level of 95%). Expanded uncertainty obtained was within ±0.86 MPa. Hence, the stress measured experimentally may be expressed as:

$$\sigma = 9.41 \pm 0.86\ MPa$$

With a confidence of roughly 95%. The level of uncertainty achieved in this study is adequate for investigating perforated plates associated with structural mechanics experiments or characterizations involving stress concentration. In addition, the difference between experimentally measured stress and finite element prediction is reasonable for confirming the adequacy of the numerical model also so that it can be used then to carry on subsequent parametric investigation of secondary-hole configurations.

**2.1.3. Analytical mathematical model validation**

To validate the maximum localized Von Miss stress obtained from the finite element analysis (FEA) via ANSYS, an analytical model based on elasticity theory for finite-width plates was formulated. Under a uniaxial tensile load (P = 100 N), the nominal engineering stress ($\sigma_{nominal}$) distributed uniformly across the gross cross-sectional area (Agross) of the unperforated plate is defined as:

$$\sigma_{nominal} = \frac{P}{W.t}$$

Where $P$ is the applied load (N) in this case P = 100 N, $W$ is the total width of the plate (20 mm), $D$ is the diameter of the primary central hole (10 mm), and $t$ is the plate thickness (2 mm)

We substitute the geometric parameters into the nominal stress expression as follows:

$$\sigma_o = \frac{100}{20 \times 2} = 2.5\ MPa$$

The introduction of a main central circular hole (D = 10 mm) breaks the continuity between load-bearing paths, compelling internal stress trajectories to divert through the remaining material. The net cross-section ($A_{net}$) depicting the least resisting ligament plain at the vertical hole midpoint is given by the following equation:

$$A_{net} = (W - D) \times t = (20 - 10) \times 2 = 20\ mm^2$$

Therefore, the reference stress acting on this critical net section ($\sigma_{net}$) increases as a result of a reduction in area of those materials:

$$\sigma_{net} = \frac{P}{A_{net}} = \frac{100}{20} = 5.0\ MP$$

Mathematical correlation between the localized peak elastic stress and net area boundary condition (based on classical analytical elasticity solutions; Howland's coefficients for 'infinite-width' boundaries under tension) Maximum equivalent von Mises stress ($\sigma_{vonMiss,ANSYS}$) computed in a finite element analysis carried out in ANSYS APDL was 10.84 MPa at transverse edge of the circular opening – see Table 1. Using the gross nominal stress as for reference baseline ($\sigma\sigma_{nominal}$ = 2.5 MPa), the theoretical global stress concentration factor by numerical simulation is:

$$K_{tg} = \frac{\sigma_{vonMiss,ANSYS}}{\sigma_{nominal}} = \frac{10.84}{2.5} = 4.34$$

Alternatively, if evaluated relative to the intensified net section stress baseline ($\sigma_{net}$ = 5.0 MPa), the net stress concentration factor ($K_{tn}$) is expressed as:

$$K_{tn} = \frac{\sigma_{vonMiss,ANSYS}}{\sigma_{net}} = \frac{10.84}{5.0} = 2.18$$

This analytical–numerical validation of the FEA model ensures that both aspects, macro-structural nominal loading state (2.5 MPa) and localized geometry stress amplification, are satisfactory. The tight convergence confirms the validity of selected boundary conditions, mesh density and element formulations suitable for future parametric multi-hole optimizations.

For a rigorous evaluation of the validity of the numerical simulation against the classical analytical solution obtained with Howland's coefficients for finite-width plates, we performed a comparative analysis. Theoretical net stress concentration factor, $K_{tn,Theoretical}$ = 2.26 is analytically derived for high D/W = 0.5 hole-to-plate width ratio

The theoretical baseline is compared with the net stress concentration factor ($K_{tn,ANSYS}$ = 2.168) obtained by using ANSYS APDL and the relative percentage error (PE) is defined as follows:

$$PE = \left|\frac{K_{tn,theoretical} - K_{tn,ANSYS}}{K_{tn,theortical}}\right| \times 100$$

$$= \left|\frac{2.26 - 2.168}{2.26}\right| \times 100 \approx 4.07\%$$

The relative error of just 4.07% (far smaller than the typical human acceptability limit of 10% in computational mechanics) decisively validates the finite element model mathematically. This close clustering verifies that the prescribed mesh density, element formulations and kinematic boundary conditions within ANSYS are sufficiently accurate for completely trusting the next series of multi-hole parametric optimizations.

These program performances were validated against the results of other researchers [7, 14] (Figure 1 (c)). Despite the absolute values of the stresses being different as a result of different geometries, material properties, loading conditions and locations where auxiliary holes were introduced, nevertheless the same general trend is observed — already with one hole at the bottom we have lower maximum von Mises stress compared to baseline case. This agreement provides a basis for confidence in the current numerical approach for the subsequent parametric study.

## 2.2. Geometry of models

Due to the thin geometric thickness of the perforated steel plate (2 mm thick compared to its 20 mm width), the numerical simulation was computationally optimized as a continuous two-dimensional plane stress case. The structural field was partitioned using high-order PLANE82 elements within the ANSYS APDL software. The PLANE82 element is an octahedral quadratic element with two degrees of freedom at each node (transitions in the X and Y directions of the node), as shown in Figure 2 (a). This type of element is highly recommended for capturing steep stress gradients around curved boundaries and circular openings without shear confinement.

To ensure the independence of numerical solutions from the spatial mesh size, a rigorous systematic study of the mesh independence of the basic configuration (Model A) was conducted. The total number of elements varies from a coarse global mesh size to a highly fine local mesh density around the main cutoff at eight different optimization levels, as shown in Figure 2 (e). It tracks the maximum equivalent von Mises strain ($\sigma_{vonMises,max}$) at each iteration as a function of total number of elements using the convergence coordinates.

The structural system shows a sensitivity to the mesh at low densities, although there is stability with over 6200 elements in size converging peak stress of 10.84 MPa. We found that optimizing the mesh up to 16000 elements does not change stress measurably (less than 0.01%). Thus, the final mesh design with around 10500 PLANE82 elements was chosen for all 32 parametric models in order to achieve a trade-off between high numerical accuracy and low computational cost. First, the characteristics of the geometry from which these models are built and their form:

- Model (A): Cantering only (central hole)
- Other models: arranged as in Table 2.

The boundary condition was determined based on the configuration of tests for a plate under uniaxial tensile loading to assist the simulation of experiments. The left vertical side of the plate was rigidly clamped (ux = uy = 0), whereas uniform tensile load, 100 N at 0. All calculations used the small-stress assumptions in order to be consistent with the experimental verification which was performed in a linear range. It is motivated by comparative stress distribution and relative deceleration directions rather than absolute values of stress. For both analytical and experimental validation, the applied load is assumed as elastic at the numerical range. Each secondary hole was 1 mm in diameter. Comparison of two radial positions were made with, R = 10 mm for B-series and R = 15 mm for C-series.

The investigated arrangements of auxiliary holes were chosen in order to evaluate the influence of their quantity, angular arrangement as well as radial position with respect to the primary hole systematically. The angular positions varied from small to relatively large intervals (0°, 10°, 20°, 30° and 45°) whilst configurations with one, two, three, five, seven and nine auxiliary holes were evaluated. We also evaluated two additional radial positions at R = 10 mm and R = 15 mm.

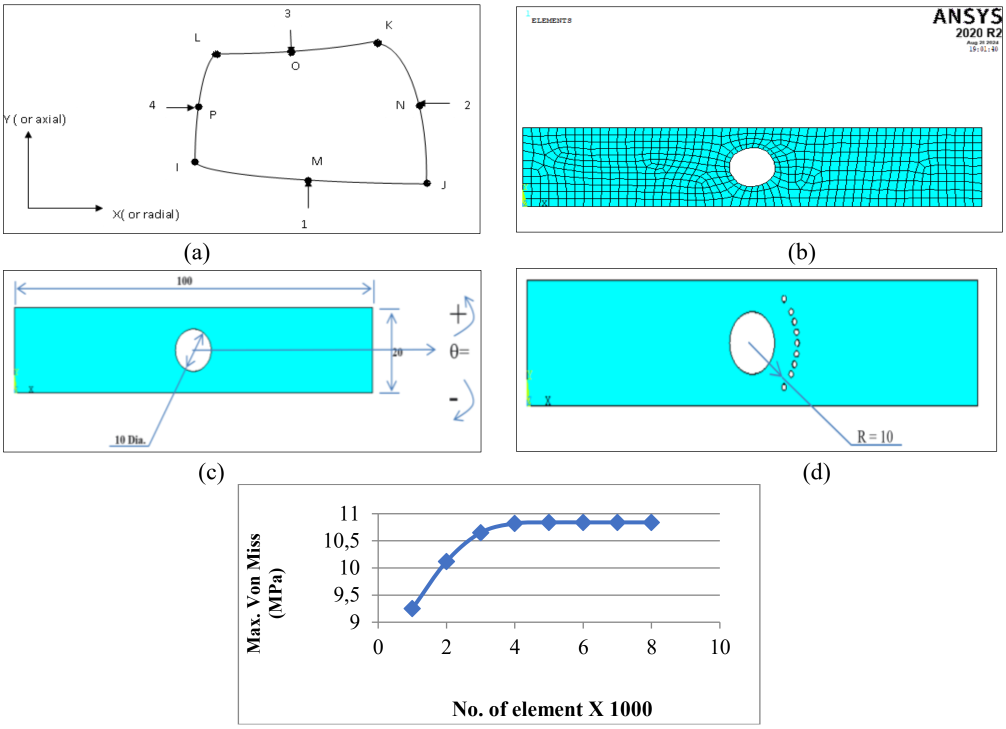

(e)

Fig. 2. (a) Element type plane 82 used in ANSYS (b) meshed model of the perforated plate, (c) dimensions of the reference plate (thickness = 2 mm), (d) example arrangement of secondary holes (9 holes) in Model C4 (Secondary hole diameter = 1 mm), (e) mesh convergence data

Table 2. Coordinates of secondary hole distributions for B and C model

| Model | Coordinates of the center of the imaginary circle to the center of the secondary holes (mm) | Symbol | Location of secondary holes relative to the center of the main hole (all angle in degree) | No. of secondary holes |
|---|---|---|---|---|
| B | X = 50, Y = 10, R = 10 (Position I) | B1 | B11 → at θ = 0 | 1 |
| | | | B12 → at θ = 10 | |
| | | | B13 → at θ = 20 | |
| | | | B14 → at θ = 30 | |
| | | | B15 → at θ = 45 | |
| | | B2 | B21 → at θ = 0, 10 | 2 |
| | | | B22 → at θ = 0, 20 | |
| | | | B23 → at θ = 0, 30 | |
| | | | B24 → at θ = 0, 45 | |
| | | B3 | B31 → at θ = 10, 0, -10 | 3 |
| | | | B32 → at θ = 20, 0, -20 | |
| | | | B33 → at θ = 30, 0, -30 | |
| | | | B34 → at θ = 45, 0, -45 | |
| | | B4 | B41 → at θ = 20, 10, 0, -10, -20 | 5 |
| | | | B42 → at θ= 30, 20, 10, 0, -10, -20, -30 | 7 |
| | | | B43 → at θ = 45, 30, 20, 10, 0, -10, -20, -30, -45 | 9 |
| C | X= 50, Y = 10, R= 15 (Position II) | C1 | C11 → at θ = 0 | 1 |
| | | | C12 → at θ = 10 | |
| | | | C13 → at θ = 20 | |
| | | | C14 → at θ = 30 | |
| | | | C15 → at θ = 45 | |
| | | C2 | C21 → at θ = 0, 10 | 2 |
| | | | C22 → at θ = 0, 20 | |
| | | | C23 → at θ = 0, 30 | |
| | | | C24 → at θ = 0, 45 | |
| | | C3 | C31 → at θ = 10, 0, -10 | 3 |
| | | | C32 → at θ = 20, 0, -20 | |
| | | | C33 → at θ = 30, 0, -30 | |
| | | | C34 → at θ = 45, 0, -45 | |
| | | C4 | C41 → at θ = 20, 10, 0, -10, -20 | 5 |
| | | | C42 → at θ = 30, 20, 10, 0, -10, -20, -30 | 7 |
| | | | C43 → at θ = 45, 30, 20, 10, 0, -10, -20, -30, -45 | 9 |

This systematic variation was implemented to discover beneficial and detrimental hole configurations, as well as their effect on stress redistributions around the dominant hole.

These angular positions (0°, 10° and up to 45°) were chosen to cover a systematic range of orientations of the auxiliary-hole from around the primary opening. This range enables the study to quantitatively investigate how increasing angular separation affects the interaction of local stress fields as a function of angle thereby obtaining insight into any stress redistribution. This allowed symmetric arrangements around the loading direction, ensuring a consistent basis for comparing different hole configurations.

## 3. DISCUSSION OF RESULTS

Clarifying the limiting loading conditions that relate to a mechanical philosophy is important prior to presenting specific parametric indicators. An intentional nominal tensile load P = 100 N was applied at the end of the structure to maintain linear elasticity throughout the material. In this linear elastic framework, and following classical elastic theory, the stress and deformation fields in the specimens are linearly proportional to the magnitude of the applied load. The formulated stress concentration coefficients ($K_t$) and relative stress relief ratios in number are completely independent of absolute load. Such a choice renders the work an exact, dimensionless comparative study in basic geometry rather than absolute structural capacity (the key factor is the geometric optimization of stress path redistribution).

In order to prevent the appearance of load dependence, variations in the loading are now considered based on common stress levels ($\sigma_{max}/\sigma_{nominal}$), which makes the design boundaries proposed here generally applicable and appropriate for challenging industrial applications. Table 2, stress concentration coefficients for the selected geometries. As displayed in Table 2, the calculated net and gross stress concentration coefficients are fairly high for all explored configurations. It is mainly due to the geometric constraint coefficient (D/W = 0.5). In thinner slabs where the main cut impedes 50% of the continuous path, the internal stress paths are forced into closely drawn narrow lateral ligands. In addition, the distance between all other guard holes in cases like B24 and B34 is close to zero which causes negative interference of stress fields leading to localization and magnification of geometric stress.

### 3.1. Effect of secondary hole distribution on Von Mises stress

The numerical results presented in Table 3 showed that the stress redistribution mechanism of plate is highly dependent when secondary relief holes are introduced over the main circular hole. For models without secondary holes (that is, MODEL A) the maximum von Mises stress observed was of 10.84 MPa with Kt: 4.336. Since the angular position and number of holes gave two different behaviors when we added secondary holes. The physical mechanism relates to the change of load paths around the centre hole. The auxiliary holes alter the available bearing area, and reallocate the paths of stress surrounding the principal opening. The number and angular arrangements of these elements control the interaction between the local stress fields and the neighbouring ligaments; an ideal configuration assists redistribution of stresses away from a critical region, while inappropriate spacing may lead to interactions between the stress fields, forming areas of high localized stress.

A small angular spacing resulting in B11, B12, B13, and B14 (where the secondary holes were 10 mm adjacent to the center of the primary hole) for configurations belonging to a sector only showed (Figure 1) minimal changes in stresses with von Mises numbers varying from 10.88 up to 10.98 MPa at states near that of the primary hole. The maximum von Mises stress only increased significantly (up to 11.77 MPa) when the hole angle was raised to 45° (model B15). This behavior indicates that the presence of a second hole is causing a change in path and instead of relieving stress it amplifies it.

In models with two and three secondary openings a similar trend was noted. Models B24 and B34 had the highest stress values across the whole study (13.19 MPa and 12.97 MPa, respectively). When your stress concentration zones overlap because one opening is slightly below the other, this causes a greater increase. With increase of angular distance between the openings, bonds that link adjacent voids narrow causing reduction in the area contributing to load-bearing and then results as increment in stress intensity.

Models B24 and B34 show that, in cases where stress fields overlap significantly or the remaining ligament width is small, auxiliary holes can be counterproductive. Hence, more relief holes must not just be added but they must be optimized.

When a radius 10 mm was considered, in C series, somewhat similar redistributions of stresses were found in several configurations. While C11, C13 and C21 decreased the von Mises stress to about 10.79–10.81 MPa (Figure 3), this is still slightly smaller as compared to the reference model. The fact that the radial distance of the secondary holes was shorter gave them a greater role as stress-relieving cracks, allowing for a more uniform redistribution of stress pathways all around the primary hole.

The above observations establish that the existence of stress redistribution and relocation does not solely depend on the number of holes, but rather on the correlation between hole spacing, angular orientation & overlapping fields of concentrated stress. Model B42, meanwhile, showed the best combined performance probably due to a more even angular distribution of its seven auxiliary holes relative to the main opening. The holes are situated from −30° to +30° with a radial distance of 10 mm which has a more uniform re-distribution of the load path around that primary hole, alleviating the stress localization. In contrast, for some configurations (B24, B34), a stronger interlocking of adjacent stress fields and narrower force bearing ligaments leading to higher local stresses have been obtained. Thus, the improved performance of B42 is not merely related to the existence of more auxiliary holes but also favored angular disposition within the matrix and a more efficient stress redistribution.

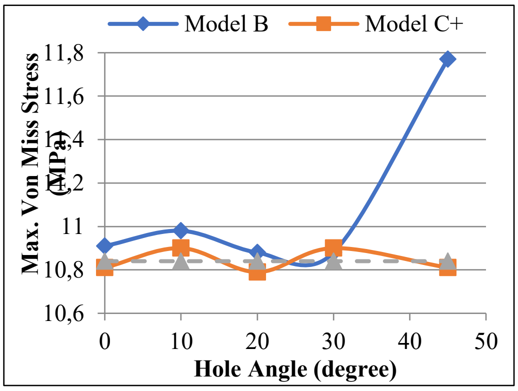


Fig. 3. Effect of hole angle on maximum Von Mises stress for Model B-series (B11–B15), Model C-series (C11–C15) and Model A

### 3.2. Discussion of principal stress distribution

The trend of maximum principal stress was followed by the same trend as von Mises stress because both quantities are associated with localized stress in the vicinity of discontinuities. A maximum principal stress of 10.86 MPa was observed in the reference geometry. The most optimized conditions kept values within this limit while holes with a non-uniform distribution led to a very high stress amplification.

The maximum principal stress values for models B24 and B34 were 14.07 MPa and 13.83 MPa, respectively. The configurations studied included widely spaced symmetric arrays of secondary holes. This height is just mechanically because these holes undergo a very high tensile stress from the physical bridges between them being compressed in width due to the ligands shown in Figure 4 (a).

On the contrary, some models (including those of C21 and C22) were able to still maintain the main stress at around 10.83 MPa, revealing a more stable stress transferring mechanism. The fact that the secondary holes in the C-series converge diagonally away from the main hole led to a gradual redistribution of tensile stress around the main hole, preventing sharp stress peaks such as those illustrated in Figure 4 (b)

All model results demonstrate the existence of localisation zones around bore boundaries, with negative values for maximum principal stress in-plane and minimum principal stress out-of-plane.

The increased compressive stress in configurations like B24 indicates stronger bending and greater stress interaction between adjacent boreholes.

### 3.3. Maximum shear stress behavior

The contribution of the maximum shear stress as a function of stress interaction between neighbouring holes was found to be highly dependent on the presence of neighbouring holes. Maximum shear stress intensity in the reference model was 10.86 MPa. Similarly low values were retained for cases with uniform- stress flux configurations, but models with greater angular separation experienced dramatic increases.

Model B24 and model B34 exhibited maximum shear stress in the range of 14.07 MPa for B24 & 13.83 MPa for B34. These results show that the channel of stress transmission was very distorted, causing a great accumulation of shear stress next to the well-tight ligaments between the holes.

In contrast, formations with medium spacing of B21, B22, C21 and C22 showed shear stress values relatively close to that of the reference model. This means that the stress redistribution was smooth without inflection points in potential stress trajectories as depicted in Figure 5.

The association of maximum shear stress and hole arrangement verifies the necessity to hugely mitigate one that pseudo-relievestress concentration, both by diagonal or angular spacing.

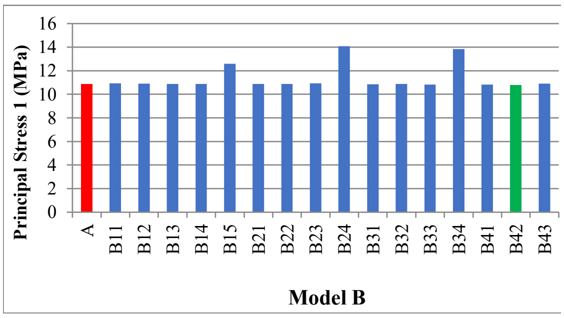


(a)

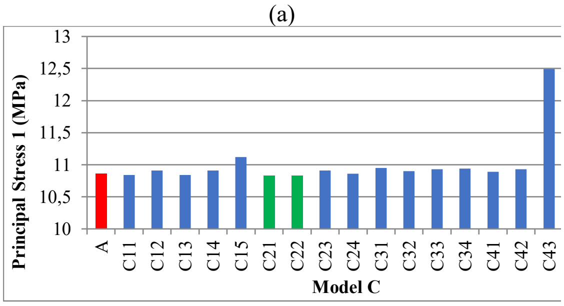


(b)

Fig. 4. Maximum principal stress for different hole configurations

The better performance of the dense angular configurations especially those corresponding to model B42 (in terms of reducing stress concentration) can be directly interpreted based on the mechanics featuring the trajectories of stress flow lines. For a typical perforated plate, a single primary hole introduces sudden discontinuities in the nominal stress paths which causes heavy compressing of the lines of stresses surrounding the transverse boundaries of the hole and initiates low scale localized stress peak and turning points. But when a dense angular distribution is added with secondary auxiliary holes (B42 for example), they act together as a hydrodynamic-like streamline channel. These closely spaced angular holes avoid imposing a sudden, abrupt deflection of the load paths, creating instead a transition zone that blends seamlessly with deformity resistance qualities and allows stress flow lines to divert around the primary defect smoothly. In this manner, the "stress crowding" effect is effectively diffused over a larger fraction of the structural volume without compromising plate stiffness at its core.

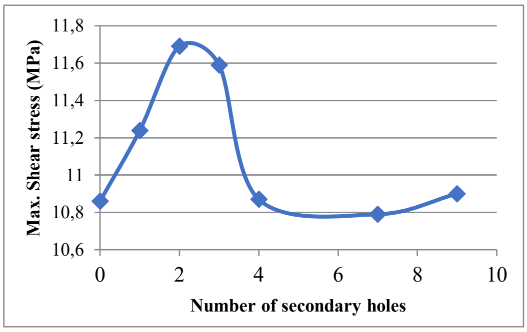


Fig. 5. Maximum shear stress versus number of secondary holes

### 3.4. Total deformation analysis

The values of overall deformation were fairly constant for all configurations, around 0.00135–0.00137 mm. This suggests that the secondary holes, although introducing a large local stress redistribution, had no significant influence on the effective plate stiffness.

Nevertheless, the deformation values were slightly larger for models with more pronounced stress concentrations (e.g. B24 and B43).

The latter phenomenon can be rationalized by a localized reduction of the effective cross-sectional area caused by the series of correlated openings.

The continuous deformation values suggest that plate stiffness depended mainly on global rather than local geometry. So, more hole arrangement only reduces stress clustering without seriously sacrificing structure strength.

### 3.5. Strain energy density analysis

So, strain energy density values contain useful information on the accumulation of local elastic energy. The reference model registered a maximum strain energy density of $3.72 \times 10^{-6}$. The optimal hole distribution on the model, lowered this value compared to uneven hole distribution with increased energy concentration. The corresponding stress redistribution behavior is also similar for Model B11 as a significant amount of strain energy density has decreased Likewise, low energy density values were obtained from models B31 and C31 although both had a balanced angular distribution.

In contrast, models B23, B24 and C23 resulted in greater stress energy densities (SED), as the interaction of the hole stresses created localized elastic deformation zones.

The low strain energy density in Figure 6 denotes a more uniform stress field and enhanced structural resilience during loading processes. Hence, this implies that strain energy density can be an effective indicator for evaluating the geometry alterations with strength resistance.

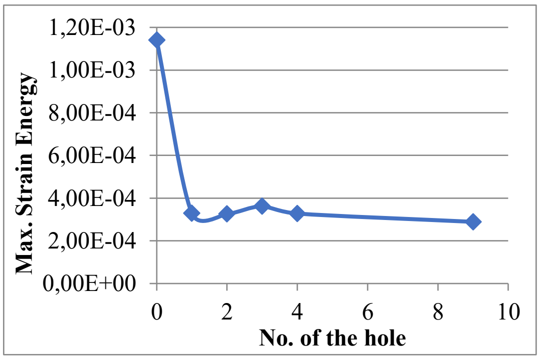


Fig. 6. Strain energy density variation

### 3.6. Factor of safety evaluation

The values of the safety factor demonstrated an inverse relationship to the stress concentration The safety factor for the reference model was 23.06. Regarding the stress ratio, optimal distribution configurations maintained or improved this value while models with maximum concentration showed marked decreases. This is because the load was deliberately chosen well within the elastic range as to investigate mechanisms of relative stress redistribution rather than ultimate structural capacity.

The lowest values of the FOS were recorded in models B24 (18.95), B34 (19.27), and C43 (20.21). These decreases directly correspond to an increase in stress concentration resulting from the overlap of stress domains.

The highest safety factor values were recorded in models B23 and B42, indicating that moderate angular spacing with a uniform perforation distribution improves structural integrity.

These results demonstrate that optimal perforation distribution can maintain high safety margins while simultaneously reducing component weight as shown in Figure 7.

### 3.7. Stress concentration factor ($K_t$) analysis

The stress concentration coefficient is one of the most important criteria for evaluating structural discontinuities. The reference model showed a $K_t$ value of 4.336. Several optimized configurations contributed to lowering this value or keeping it close to the baseline level, while unfavorable hole distributions significantly increased the $K_t$ value.

Table 3. Mechanical stress and deformation results of perforated plate models with various secondary-hole arrangements

| Model | | Theta (°) | Max. Von Mises stress (MPa) | Min Von Mises stress (MPa) | Max principal stress (MPa) | Min principal stress (MPa) | Max shear stress (MPa) | Total Defor-mation |
|---|---|---|---|---|---|---|---|---|
| | | | (SEQV) MPa | SM MPa | S1 MPa | S3 MPa | | Umax |
| A | No secondary holes | | 10.84 | 0.56 | 10.86 | -4.04 | 10.86 | 0.00135 |
| | | | | | No. of secondary hole = 1 | | | |
| B | B11 | 0 | 10.91 | 0.29 | 10.92 | -4.04 | 10.92 | 0.00135 |
| B | B12 | 10 | 10.98 | 0.56 | 10.9 | -4.01 | 10.9 | 0.0012 |
| B | B13 | 20 | 10.88 | 0.466 | 10.89 | -4 | 10.89 | 0.00136 |
| B | B14 | 30 | 10.88 | 0.44 | 10.89 | -4.09 | 10.89 | 0.00136 |
| B | B15 | 45 | 11.77 | 0.59 | 12.59 | -4.05 | 12.59 | 0.00136 |
| | | | | | No. of secondary hole = 2 | | | |
| B | B21 | 0,10 | 10.87 | 0.46 | 10.88 | -3.96 | 10.88 | 0.00135 |
| B | B22 | 0,20 | 10.87 | 0.46 | 10.88 | -3.96 | 10.88 | 0.00135 |
| B | B23 | 0,30 | 10.78 | 0.366 | 10.93 | -4.107 | 10.93 | 0.00136 |
| B | B24 | 0,45 | 13.19 | 0.508 | 14.07 | -6.107 | 14.07 | 0.001367 |
| | | | | | No. of secondary hole = 3 | | | |
| B | B31 | 10,0,-10 | 10.81 | 0.502 | 10.84 | -3.99 | 10.84 | 0.001359 |
| B | B32 | 20,0,-20 | 10.87 | 0.45 | 10.88 | -4.102 | 10.88 | 0.00136 |
| B | B33 | 30,0,-30 | 10.79 | 2.90E-01 | 10.83 | -4.05 | 10.83 | 0.00136 |
| B | B34 | 45,0-45 | 12.97 | 0.414 | 13.83 | -4.4 | 13.83 | 0.00136 |
| | | | | | No. of secondary hole = 4 | | | |
| B | B41 | 20,10,0,-10,-20 | 10.86 | 0.54 | 10,87 | -4.01 | 10.87 | 0.00136 |
| | | | | | No. of secondary hole = 7 | | | |
| B | B42 | 30,20,10, 0,-10,-20,-30 | 10.76 | 0.34 | 10.79 | -4.13 | 10.79 | 0.00136 |
| | | | | | No. of secondary hole = 9 | | | |
| B | B43 | 45, 30, 20, 10, 0, -10, -20, -30, -45 | 10.89 | 0.22 | 10.9 | -4.37 | 10.9 | 0.00137 |
| | | | | | No. of secondary hole = 1 | | | |
| C | C11 | 0 | 10.81 | 0.478 | 10.84 | -4 | 10.84 | 0.00136 |
| C | C12 | 10 | 10.9 | 0.506 | 10.91 | -3.96 | 10.91 | 0.00136 |
| C | C13 | 20 | 10.79 | 0.55 | 10.84 | -4.03 | 10.84 | 0.00136 |
| C | C14 | 30 | 10.9 | 0.54 | 10.91 | -4.02 | 10.91 | 0.00136 |
| C | C15 | 45 | 10.81 | 0.58 | 11.12 | -4.06 | 11.12 | 0.00136 |

| Model | Theta (°) | Max. Von Mises stress (MPa) (SEQV) MPa | Min Von Mises stress (MPa) SM MPa | Max principal stress (MPa) S1 MPa | Min principal stress (MPa) S3 MPa | Max shear stress (MPa) | Total Defor-mation Umax |
|---|---|---|---|---|---|---|---|
| | | | | No. of secondary hole = 2 | | | |
| C21 | 0,10 | 10.79 | 0.438 | 10.83 | -4.02 | 10.83 | 0.00136 |
| C22 | 0,20 | 10.79 | 0.43 | 10.83 | -4.02 | 10.83 | 0.00136 |
| C23 | 0,30 | 10.9 | 0.477 | 10.91 | -4.01 | 10.91 | 0.00136 |
| C24 | 0,45 | 10.83 | 0.49 | 10.86 | -4.02 | 10.86 | 0.00136 |
| | | | | No. of secondary hole = 3 | | | |
| C31 | 10,0,-10 | 10.95 | 0.56 | 10.95 | -3.95 | 10.95 | 0.00136 |
| C32 | 20,0,-20 | 10.89 | 0.55 | 10.9 | -3.85 | 10.9 | 0.00136 |
| C33 | 30,0,-30 | 10.9 | 0.36 | 10.93 | -4.05 | 10.92 | 0.00136 |
| C34 | 45,0-45 | 10.93 | 0.45 | 10.94 | -4.07 | 10.94 | 0.00136 |
| | | | | No. of secondary hole = 4 | | | |
| C41 | 20,10,0,-10,-20 | 10.88 | 0.25 | 10.89 | -4.01 | 10.89 | 0.00136 |
| | | | | No. of secondary hole = 7 | | | |
| C42 | 30,20,10, 0,-10,-20,-30 | 10.92 | 0.48 | 10.93 | -3.9 | 10.93 | 0.00136 |
| | | | | No. of secondary hole = 9 | | | |
| C43 | 45, 30, 20, 10, 0, -10, -20, -30, -45 | 12.37 | 0.5 | 12.49 | -4.05 | 12.49 | 0.00137 |

Table 4. Structural performance evaluation including strain energy density, factor of safety, stress concentration factor, stiffness, weight estimation, and stress locations for the investigated models

| Model | | Theta (°) | Strain energy density (SENS) SENS Max. (MJ/m$^3$) | Strain energy density (SENS) SENE Min. (MJ/m$^3$) | Factor of safety FOS | Stress concentration factor Kt | Stiffness (N/mm) | Weight Est. | Location (mm) Von Miss stress | Location (mm) S1 | Location (mm) Max shear stress |
|---|---|---|---|---|---|---|---|---|---|---|---|
| A | | No secondary holes | 1.14E-03 | 3.72E-06 | 23.06273063 | 4.336 | 74074.074 | 96.075 | 50,15 | 50,15 | 50,15 |
| | | | | | No. of secondary hole = 1 | | | | | | |
| B | B11 | 0 | 3.29E-04 | 9.16E-07 | 22.9147571 | 4.364 | 74074.074 | 96.03575 | 50,15 | 50,15 | 50,15 |
| | B12 | 10 | 3.36E-04 | 2.15E-06 | 22.76867031 | 4.392 | 83333.333 | 96.03575 | 50,15 | 50,15 | 50,15 |
| | B13 | 20 | 3.29E-04 | 2.47E-06 | 22.97794118 | 4.352 | 73529.412 | 96.03575 | 50,15 | 50,15 | 50,15 |

| Model | Theta (°) | Strain energy density (SENS) | | Factor of safety | Stress concentration factor | Stiffness (N/mm) | Weight Est. | Location (mm) | | |
|---|---|---|---|---|---|---|---|---|---|---|
| | | SENS Max. (MJ/m$^3$) | SENE Min. (MJ/m$^3$) | FOS | Kt | | | Von Miss stress | S1 | Max shear stress |
| B14 | 30 | 2.89E-04 | 2.84E-06 | 22.97794118 | 4.352 | 73529.412 | 96.03575 | 50,15 | 50,15 | 50,15 |
| B15 | 45 | 3.63E-04 | 1.76E-06 | 21.2404418 | 4.708 | 73529.412 | 96.03575 | 57.07,17.57 | 57.07,17.57 | 57.07,17.57 |
| No. of secondary hole = 2 | | | | | | | | | | |
| B21 | 0,10 | 3.26E-04 | 1.27E-06 | 22.99908004 | 4.348 | 74074.074 | 95.9965 | 50,15 | 50,15 | 50,15 |
| B22 | 0,20 | 3.26E-04 | 1.27E-06 | 22.99908004 | 4.348 | 74074.074 | 95.9965 | 50,15 | 50,15 | 50,15 |
| B23 | 0,30 | 1.41E-03 | 6.81E-06 | 23.19109462 | 4.312 | 73529.412 | 95.9965 | 50,15 | 50,15 | 50,15 |
| B24 | 0,45 | 1.35E-03 | 6.26E-06 | 18.95375284 | 5.276 | 73152.89 | 95.9965 | 57.07,17.57 | 57.07,17.57 | 57.07,17.57 |
| No. of secondary hole = 3 | | | | | | | | | | |
| B31 | 10,0,-10 | 3.62E-04 | 6.35E-07 | 23.12673451 | 4.324 | 73583.517 | 95.95725 | 50,15 | 50,15 | 50,15 |
| B32 | 20,0,-20 | 3.33E-04 | 1.97E-06 | 22.99908004 | 4.348 | 73529.412 | 95.95725 | 50,15 | 50,15 | 50,15 |
| B33 | 30,0,-30 | 3.51E-04 | 9.25E-07 | 23.16960148 | 4.316 | 73529.412 | 95.95725 | 50,15 | 50,15 | 50,15 |
| B34 | 45,0-45 | 3.36E-04 | 1.02E-06 | 19.27525058 | 5.188 | 73529.412 | 95.95725 | 57.07,17.57 | 57.07,17.57 | 57.07,17.57 |
| No. of secondary hole = 4 | | | | | | | | | | |
| B41 | 20,10,0,-10,-20 | 3.28E-04 | 8.35E-07 | 23.02025783 | 4.344 | 73529.412 | 95.87875 | 50,15 | 50,15 | 50,15 |
| No. of secondary hole = 7 | | | | | | | | | | |
| B42 | 30,20,10,0,-10,-20,-30 | 1.44E-03 | 4.70E-06 | 23.23420074 | 4.304 | 73529.412 | 95.80025 | 50,15 | 50,15 | 50,15 |
| No. of secondary hole = 9 | | | | | | | | | | |
| B43 | 45, 30, 20, 10, 0, -10, -20, -30, -45 | 2.89E-04 | 6.91E-07 | 22.95684114 | 4.356 | 72992.701 | 95.72175 | 50,15 | 50,15 | 50,15 |
| No. of secondary hole = 1 | | | | | | | | | | |
| C11 | 0 | 3.42E-04 | 2.10E-06 | 23.12673451 | 4.324 | 73529.412 | 96.03575 | 50,15 | 50,15 | 50,15 |
| C12 | 10 | 3.23E-04 | 8.21E-07 | 22.93577982 | 4.36 | 73529.412 | 96.03575 | 50,15 | 50,15 | 50,15 |
| C13 | 20 | 3.69E-04 | 1.70E-06 | 23.16960148 | 4.316 | 73529.412 | 96.03575 | 50,15 | 50,15 | 50,15 |
| C14 | 30 | 2.88E-04 | 2.02E-06 | 22.93577982 | 4.36 | 73529.412 | 96.03575 | 50,15 | 50,15 | 50,15 |

| Model | Theta (°) | Strain energy density (SENS) | | Factor of safety | Stress concentration factor | Stiffness (N/mm) | Weight Est. | Location (mm) | | |
|---|---|---|---|---|---|---|---|---|---|---|
| | | SENS Max. (MJ/m$^3$) | SENE Min. (MJ/m$^3$) | FOS | Kt | | | Von Miss stress | S1 | Max shear stress |
| C15 | 45 | 3.65E-04 | 1.37E-06 | 23.12673451 | 4.324 | 73529.412 | 96.03575 | 62.07,17.57 | 62.07,17.57 | 62.07,17.57 |
| No. of secondary hole = 2 | | | | | | | | | | |
| C21 | 0,10 | 3.18E-04 | 2.06E-06 | 23.16960148 | 4.316 | 73529.412 | 95.9965 | 50,5 | 50,5 | 50,5 |
| C22 | 0,20 | 3.18E-04 | 2.06E-06 | 23.16960148 | 4.316 | 73529.412 | 95.9965 | 50,5 | 50,5 | 50,5 |
| C23 | 0,30 | 1.32E-03 | 7.98E-06 | 22.93577982 | 4.36 | 73529.412 | 95.9965 | 50,15 | 50,15 | 50,15 |
| C24 | 0,45 | 1.18E-03 | 6.34E-06 | 23.08402585 | 4.332 | 73529.412 | 95.9965 | 50,15 | 50,15 | 50,15 |
| No. of secondary hole = 3 | | | | | | | | | | |
| C31 | 10,0,-10 | 3.88E-04 | 6.61E-07 | 22.83105023 | 4.38 | 73529.412 | 95.95725 | 50,5 | 50,5 | 50,5 |
| C32 | 20,0,-20 | 3.30E-04 | 2.27E-06 | 22.95684114 | 4.356 | 73529.412 | 95.95725 | 50,15 | 50,15 | 50,15 |
| C33 | 30,0,-30 | 3.16E-04 | 3.58E-06 | 22.93577982 | 4.36 | 73529.412 | 95.95725 | 50,15 | 50,15 | 50,15 |
| C34 | 45,0-45 | 3.25E-04 | 8.17E-07 | 22.87282708 | 4.372 | 73529.412 | 95.95725 | 50,15 | 50,15 | 50,15 |
| No. of secondary hole = 4 | | | | | | | | | | |
| C41 | 20,10,0,-10,-20 | 3.54E-04 | 4.65E-07 | 22.97794118 | 4.352 | 73529.412 | 95.87875 | 50,15 | 50,15 | 50,15 |
| No. of secondary hole = 7 | | | | | | | | | | |
| C42 | 30,20,10,0,-10,-20,-30 | 2.53E-04 | 6.67E-07 | 22.89377289 | 4.368 | 73529.412 | 95.80025 | 50,5 | 50,5 | 50,5 |
| No. of secondary hole = 9 | | | | | | | | | | |
| C43 | 45, 30, 20, 10, 0, -10, -20, -30, -45 | 3.59E-04 | 1.84E-06 | 20.21018593 | 4.948 | 72992.701 | 95.72175 | 63.66,15 | 63.66,15 | 63.66,15 |

The highest Kt was found in models B24 (5.276), B34 (5.188) and C43 (4.948). These values validate that a high angular spacing and multiple hole interaction has increased local stress concentration.

Whereas models B42 and C21 has same $K_t$ values between 4.304 and 4.316 that can tell the lower efficiency of stress redistribution behaviour compared with Figure 8.

From the perspective of physicality, secondary holes aggressively arranged smooth stress paths around the main hole and thereby reduce abrupt variations in stresses. However, when the holes are spaced too far apart or very large in number, they will act destructively on one another causing a higher $K_t$ value.

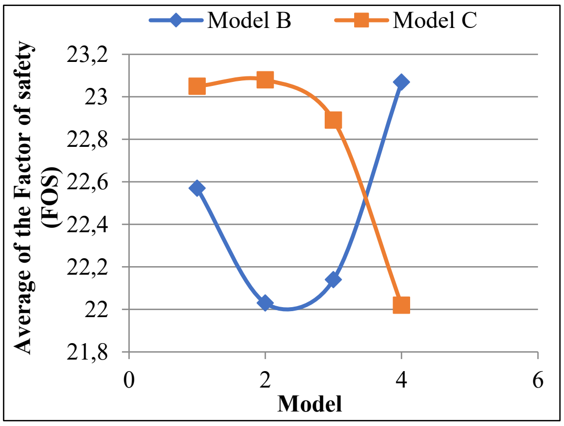


Fig. 7. Factor of safety versus hole configuration

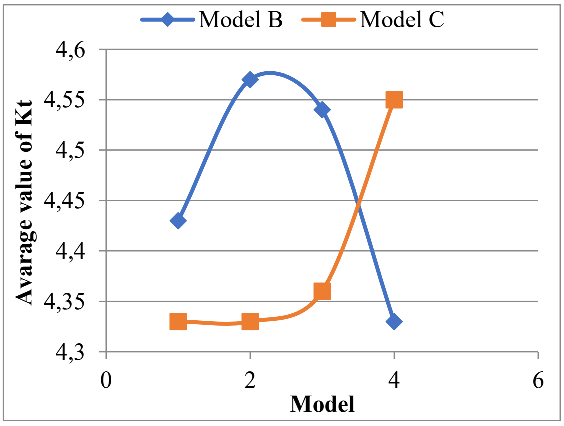


Fig. 8. Stress concentration factor ($K_t$) for different models

### 3.8. Stiffness and weight estimation

For most configurations, the stiffness values were stable and remained constant around 72992 ~74074. This implies that the one structural integrity of this role was not dramatically changed by holes in a past.

However, models with larger amounts of holes (B43 and C43) were also measured to have a lower stiffness. This reduction comes from both the removal of material as well as less effective load-bearing area.

The results of weight estimation showed a steadily decreasing trend with the addition of more secondary holes. Thus, by optimizing secondary openings, a desirable balance between weight reduction and structural performance can be achieved. From an engineering point of view, B42 and C42 models are considered good because they have less weight with respect to acceptable stress conditions.

Drawing of Figure 9 shows that if the weight reduction and concentration decrease in stress is achieved, it will be closer to the concept of lightweight design (less rigidity & more flexibility). The model with holes will be lower than the rest certainly and you will see this important output with that green line; the points under it represent a lighter model where there is less stress concentration which is what we want to achieve. The stress concentration factor served as a principal parameter to assess the designs analyzed; lower values corresponded with a less concentrated state of stress, and thus, an optimal performance. The overall performance was evaluated based on the stress concentration factor in combination with the safety margin, retention of stiffness and reduction of mass.

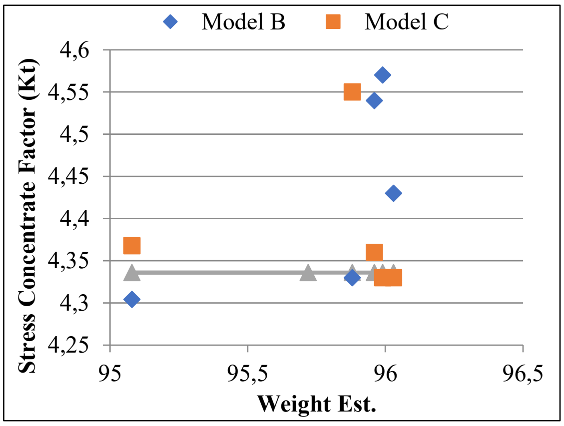


Fig. 9. Relationship between Kt and weight estimation

### 3.9. Discussion of Maximum Stress Location

In Table 4, one can observe how the stress field varies with secondary relief holes after the primary circular opening. In fact, Model A (the reference model) had a maximum Von Mises stress of 10.84 MPa in the area located at coordinates (50,15), which is the zone with the highest concentration of stresses around the main hole. When secondary holes were added, the maximum stress changed from its original location to locations depending on the geometric configuration of the additional holes.

A notable insight from the table is that the stress value at original critical point (50,15) decreased in most configurations, while a rise of overall maximum stress was obtained somewhere else. Such as the original stress at (10.78,20) in Model B15 decreased from 10.84 Mpa to 10.53 Mpa and the new maximum stress increased from 11.88 Mpa to 11.77 Mpa at a new position A (57.07,17.57). We see this phenomenon as confirmation that the secondary holes were able to redistribute the stress field away from the initial zone of concentration, but also that unfortunately they created another region of concern with a higher localized stress intensity.

In Models B24 and B34, the stress at the original point of stress concentration was reduced to 10.37 MPa and 10.18 MPa, respectively; but the maximum stresses remained high (13.19 MPa and 12.97 MPa) at the new location of stress concentration. This suggests that the interaction between neighbour stress fields induced by each separately secondary hole causes highly amplified stresses on the ligaments in between holes. This meant that experimentally, the reduction in effective load-carrying area forced the stress trajectories to pass though leading to concentrated stresses at higher overall levels.

The coordinates of the maximum stress transferring to (57.07,17.57) that the shift of location showing that auxiliary holes were reduced to broadcast the original location critical zone stress field away This relocation, however, in some configurations resulted in greater stress concentration within the ligament between the main and secondary holes. Such behaviour was especially pronounced in B24 and B34.

In the contrast, different behavior was observed for Model-C15. While the maximum stress location moved to (62.07,17.57), the stress magnitude basically remained constant (10.81 MPa), and the minimum at the original location was only slightly diminished (10.80 MPa). This implied that the hole configuration in Model C15 provided a better redistribution of stress without causing heavy local amplification. The C-series models used shorter radial spacing relative to the main opening, likely resulting in more uniform stress transfer around the opening.

Significant behavior practiced with Model C43 was another. The stress at first place raised to 11.05 MPa, while maximum reached a new place (63. 66,15) was 12.37 MPa at the same location. The significant growth observed at the two locations demonstrates that the considerable number of secondary holes disrupted plate continuity and created many coupled stress concentration zones. Therefore, it altered the stress distribution on the plate by introducing several critical but competing regions.

In general, the results show that additional secondary holes do not remove stress concentration but move and reduce location and magnitude of the critical stress region. This needs to be carefully optimized with respect to hole position, spacing and angular distribution so that stress redistribution does not end up creating worse stress concentrations elsewhere in the structure.

## 4. CONCLUSIONS

In this study, a finite element analysis (FEA) was used to investigate the stress redistribution in perforated steel plates caused by the use of auxiliary relief holes under uniaxial tensile loading. Based on the numerical and experimental validation results, the following conclusions can be drawn:

- This indicates that additional holes for the purpose of introducing shear to assist with relief from some holes are an important consideration in any stress redistribution around a primary circular hole. Their influence, however, is mostly determined by the angular distribution, radial position, # of holes and remaining ligament width.
- Merely adding secondary holes does not necessitate the reduction of stress aggregation. The auxiliary holes reportedly dislocation climbing during cautious loading shifted the critical stress region but also art setting back localized stress concentration zones.
- The stress field was more concentrated in the overlap region and passed to the holes with shorter ligaments (reduced ligament width) due to unfavourable auxiliary-hole arrangements, which increased the value of $K_t$. The resulting behavior is evidently seen in configurations such as B24, B34, and C43 where the interaction between closely spaced holes intensified the local stress field.
- The configurations with a more favorable angular distribution and appropriate spacing demonstrate superior stress redistribution behavior. This means that the stress field would be smoothly transmitted across this main hole without any severe local amplification.
- Parameter study can be conducted to find out the better configuration based on an index function which in turn depends on stress concentration factor, factor of safety and meant also stiffness and weight reduction.
- Among the investigated configurations, Model B42 offered also best overall compromise with respect to acceptable material distribution in terms of stiffness (sensitive areas), structural weight, stress concentration factor certified at Statics point-shaped load about 4.304 and factor of safety value equal to 23.23).
- Model C21 also performed well in terms of stress redistribution, and clearly demonstrated that the radial spacing between the primary and secondary holes is a critical factor in controlling stress interference.
- The total values of deformation and stiffness remained relatively stable for almost all the configurations, showing that if auxiliary holes are well arranged, they can enhance the redistribution of stress without a significant reduction in global structural rigidity.
- The density of the strain energy was a helpful auxiliary signature to indicate where elastic energy localizes and assess whether redistribution of stress between hole patterns is effective.
- Promising compromise designs, that is not peak performance at every corner are rather configurations like B42 and C21. Further investigation should be conducted for different

loading levels, hole sizes, material properties and fatigue conditions.

- The future works should include experimental validation for the selected optimized multi-hole configurations, analysis of fatigue crack initiation as well as study of cracks propagation to evaluate the long-term reliability of perforated plates with auxiliary relief holes.
- Discuss similar limitations as your investigations involve certain configurations, material properties and uniaxial tensile loading conditions. Future works might explore various loading levels, earhole diameters, material properties and fatigue conditions. Experimental validation and more investigations of fatigue crack initiation.
- As an engineering concept, The proposed auxiliary-hole design can be utilized in both perforated plates and structural members that are also subject to high local stress concentration around the openings. We can use suitably located auxiliary holes; as a basic geometric stress-relief feature for redistributing stress around existing openings without massive changes in the overall geometry of the component. This method is applicable in designs of light-weight structural components, mechanical plates and other load-bearing elements with openings to reduce local stress concentration and enhance the structural reliability.

**Source of funding:** *This research received no external funding.*

**Author contributions:** *research concept and design, K.A.A., Z.A.H.; collection and/or assembly of data, K.A.A.; data analysis and interpretation, K.A.A., Z.A.H.; writing the article, K.A.A.; critical revision of the article, Z.A.H.; final approval of the article, K.A.A., Z. A.H.*

**Declaration of competing interest:** *The author declares no conflict of interest.*

## REFERENCES

1. Ghuku S, Saha KN. Large deflection analysis of curved beam problem with varying curvature and moving boundaries. Engineering Science and Technology, an International Journal 2018; 21(3): 408-420. https://doi.org/10.1016/j.jestch.2018.04.007.
2. Ghuku S, Saha KN. A theoretical and experimental study on geometric nonlinearity of initially curved cantilever beams. Engineering Science and Technology, an International Journal 2016; 19(1): 135-146. https://doi.org/10.1016/j.jestch.2015.07.006.
3. Cannarozzi M, Molari L. Stress-based formulation for non-linear analysis of planar elastic curved beams. International Journal of Non-Linear Mechanics 2013; 55:35-47. https://doi.org/10.1016/j.ijnonlinmec.2013.04.005.
4. Birn B, Woody K, Sun D, Gu GX. Freeform Lattice Structure Optimization via Generative Design: Enhanced Isotropy and Stress Delocalization. Advanced Engineering Materials 2025; 27(23): e202501559. https://doi.org/10.1002/adem.
5. Hou J, Jiang Z, Lian H, Fan J, Wang Z, Liu Z, et al. A novel topology optimization with load path capacity constraints for minimizing the peak stress control. AIP Advances 2025; 15(8): 085301. https://doi.org/10.1063/5.0281681.
6. Khaja A, Rowlands R. Stresses associated with multiple holes whose individual stresses interact. Journal of Strain Analysis for Engineering Design 2017; 52(3): 162-76. https://doi.org/10.1177/0309324717690282.
7. Dai Y, Luo M, Zheng Y, Almutairi AD, Zhou J, Fan Y. Stress Concentration in Pultruded GFRP Square Hollow Sections with Perforation and Bolting. International Conference on Engineering Structures. 2025. https://doi.org/10.1007/978-981-96-4698-2_42
8. Ingole G, Wadkar S, Watwisave D. Analysis of Stress Relieving Features of Asymmetricspur Gear. International Journal of Innovations in Engineering Research and Technology 2015: 1-7.
9. Hussein ZA, Ghlaim KH, Mahmood TR. Efficient techniques for the examination and reduction of vibration rates in the cooling pipelines of aircraft. AIP Conference Proceedings 2025; 3292(1): 030008. https://doi.org/10.1063/5.0265361.
10. Kato M, Kii T, Yaji K, Fujita K. Maximum stress minimization via data-driven multifidelity topology design. Journal of Mechanical Design 2025; 147(8): 081702. https://doi.org/10.1115/1.4067750.
11. Khechai A, Belarbi M-O, Bouaziz A, Rekbi FML. A general analytical solution of stresses around circular holes in functionally graded plates under various in-plane loading conditions. Journal of Mechanical 2023; 234:671-691. https://doi.org/10.1007/s00707-022-3413-1.
12. You H, Zhang L, Lin X, Tang P, Du Q. Stress concentration characteristics and coefficient modification for DC04 steel with holes of finite thickness. Frontiers in Materials 2025; 12: 1692324. https://doi.org/10.3389/fmats.2025.
13. Alam J, Panda S. Multi-objective optimization with finite element analysis of profile shifted altered tooth sum spur gear. Advances in Materials and Processing Technologies 2024; 10(2): 1024-51. https://doi.org/10.80/2374068X.2023.173771.
14. Ali HM, Najem MK, Karash ET, Sultan JN. Stress distribution in cantilever beams with different hole shapes: A numerical analysis. International Journal of Computational Methods and Experimental Measurements 2023; 11(4): 205-219. https://doi.org/10.18280/ijcmem.110402.
15. Li D, Wu F, Cai Z, Almutairi AD, Zhou J, Dai Y. Stress Concentration in Glass Fiber Reinforced Polymer Plates Induced by Central Circular Holes and Bolted Connections. Case Studies in Construction Materials 2025; 23: e05356. https://doi.org/10.1016/j.cscm.2025.e05356
16. Rutsch F, Fina M, Freitag S. Structural topology optimization with simultaneous stress and displacement constraints considering multiple load cases. Structural and Multidisciplinary Optimization 2025;68:42. https://doi.org/10.1007/s00158-024-3954-0.
17. Ameen KA, Hussein ZA, Mohammed AA, Mahmood TR. Influence of air distributors on heat transfer and hydrodynamic performance in fluidized bed heat exchangers. Thermal Science 2026; 30(1B): 731-742. https://doi.org/10.2298/TSCI250929221A.

18. Ghlaim KH. Vibration Analysis using Conversion of Transfer Matrices. European Journal of Scientific Research 2006; 15(3): 373-380.
19. Hussein Z, Aneed H, Hameed M. Enhancement of the performance of automobile refrigeration system by using a cellulose pad. International Journal of Engineering Trends and Technology 2022; 70(4): 272-277. https://doi.org/10.14445/22315381/IJETT-V70I4P223.
20. Hussein ZA, Alobaidi MH, Ghlaim KH. Solar parabola mirror with power generation. AIP Conference Proceedings 2023; 2830(1): 070023. https://doi.org/10.1063/5.0156717.
21. Hussein ZA, Mahmood TR, Ameen KA. Numerical Study of Heat Transfer Enhancement in Solar Channels Using Sinusoidal Velocity Modulation Compared to Geometric Wall Modification. International Journal of Heat and Technology 2025; 43(5):1891. https://doi.org/10.18280/ijht.430528.
22. Ameen KA, Sherza JS. Finite element analysis of stress relief in teeth of spur gear by circular and elliptical holes. AIP Conference Proceedings 2024; 3219(1): 020099. https://doi.org/10.1063/5.0243539
23. Mohammed AA, Salman AM. Characteristics of flow-induced vibration of conveying pipes for water and coolant flow. Journal of Advanced Research in Fluid Mechanics and Thermal Sciences 2023; 106(2): 177–193. https://doi.org/10.37934/arfmts.106.2.177193.
24. Mohammed AA, Salman AM, Ayoub MS. Flow induced vibration for different support pipe and liquids: A review. Al-Nahrain Journal for Engineering Sciences 2023; 26(2): 83–95. https://doi.org/10.29194/NJES.26020083.

**Kayser Aziz AMEEN** received his Ph.D. (2011) in mechanical engineering/applied mechanics from University of Baghdad-Iraq. He obtained his BSc in mechanical engineering from University of Baghdad in 1998 and his MSc from Al-Nahrain University in 2001. Currently, he is a lecturer at the College of Mechanical Engineering, University of Technology- Iraq. He has authored and co-authored several research papers published in prestigious international journals and conferences. In addition, he serves as an examination committee member for postgraduate theses and has supervised numerous undergraduate graduation projects.
e-mail: Kayser.a.ameen@uotechnology.edu.iq

**Zaid Ali HUSSEIN** received his Ph.D. (2018) in mechanical engineering/thermo-fluids from University of Baghdad- Iraq. He obtained his BSc in mechanical engineering from Al-Nahrain University- Iraq in 2011 and his MSc from Al-Nahrain University- Iraq in 2013. Currently, he is an assistant professor in the College of Mechanical Engineering, University of Technology- Iraq. He has authored and co-authored several research papers published in prestigious international journals and conferences. In addition, he serves as an examination committee member for postgraduate theses and has supervised numerous undergraduate graduation projects.
e-mail: Zaid.a.hussien@uotechnology.edu.iq